

This is a repository copy of *Heterogeneity of grain boundary properties in Cu₂ZnSnS₄:A first-principles study*.

White Rose Research Online URL for this paper:

<https://eprints.whiterose.ac.uk/199838/>

Version: Published Version

Article:

Hao, Ning Jing, Ding, Rui Xue, Tong, Chuan Jia et al. (1 more author) (2023)

Heterogeneity of grain boundary properties in Cu₂ZnSnS₄:A first-principles study. *Journal of Applied Physics*. 145002. ISSN 1089-7550

<https://doi.org/10.1063/5.0147435>

Reuse

This article is distributed under the terms of the Creative Commons Attribution (CC BY) licence. This licence allows you to distribute, remix, tweak, and build upon the work, even commercially, as long as you credit the authors for the original work. More information and the full terms of the licence here:


<https://creativecommons.org/licenses/>

Takedown

If you consider content in White Rose Research Online to be in breach of UK law, please notify us by emailing eprints@whiterose.ac.uk including the URL of the record and the reason for the withdrawal request.

RESEARCH ARTICLE | APRIL 12 2023

Heterogeneity of grain boundary properties in $\text{Cu}_2\text{ZnSnS}_4$: A first-principles study

Ning-Jing Hao; Rui-Xue Ding; Chuan-Jia Tong ; ... et. al



Journal of Applied Physics 133, 145002 (2023)

<https://doi.org/10.1063/5.0147435>



CrossMark

Articles You May Be Interested In

Pressure-induced structural and electronic transitions in kesterite-type $\text{Cu}_2\text{ZnSnS}_4$

Journal of Applied Physics (August 2018)

Structural transitions of ordered kesterite-type $\text{Cu}_2\text{ZnSnS}_4$ under pressure

Appl. Phys. Lett. (January 2017)

Epitaxial growth of $\text{Cu}_2\text{ZnSnS}_4$ thin film on Si by radio frequency magnetron sputtering

Appl. Phys. Lett. (March 2020)

AIP Advances

Why Publish With Us?

-  **25 DAYS**
average time to 1st decision
-  **740+ DOWNLOADS**
average per article
-  **INCLUSIVE**
scope

[Learn More](#)

Heterogeneity of grain boundary properties in $\text{Cu}_2\text{ZnSnS}_4$: A first-principles study

Cite as: J. Appl. Phys. 133, 145002 (2023); doi: 10.1063/5.0147435

Submitted: 22 February 2023 · Accepted: 25 March 2023 ·

Published Online: 12 April 2023



View Online



Export Citation



CrossMark

Ning-Jing Hao,¹  Rui-Xue Ding,¹  Chuan-Jia Tong,^{1,2,a)}  and Keith P. McKenna^{2,a)} 

AFFILIATIONS

¹Hunan Key Laboratory of Nanophotonics and Devices, Hunan Key Laboratory of Super-Microstructure and Ultrafast Process, School of Physics and Electronics, Central South University, Changsha 410083, China

²School of Physics, Engineering and Technology, University of York, Heslington, York YO10 5DD, United Kingdom

^{a)}Authors to whom correspondence should be addressed: keith.mckenna@york.ac.uk and chuanjia.tong@csu.edu.cn

ABSTRACT

Using first-principles density functional calculations, we investigate the structure and properties of previously unstudied grain boundaries (GBs) in the solar absorber material copper-zinc-tin-sulfide (CZTS). We identify four stable low- Σ value symmetric tilt GBs with low formation energies: $\Sigma 3$ (111) and $\Sigma 5$ (201), each with two different GB terminations. Compared to CdTe and CuInSe, GBs in the quaternary semiconductor CZTS exhibit a wider variety of electronic states due to the more complex chemical environment near the GB, including under-coordinated atoms and dangling bonds. Further analysis confirms that strong dangling bonds introduce deep gap states in all GBs studied. We also investigate segregation and electronic properties of intrinsic point defects to GBs and find that one of the $\Sigma 3$ (111) GBs exhibits an abnormal defect segregation behavior that favors Cu-poor (Zn-rich) GB composition, which is beneficial for its overall performance.

© 2023 Author(s). All article content, except where otherwise noted, is licensed under a Creative Commons Attribution (CC BY) license (<http://creativecommons.org/licenses/by/4.0/>). <https://doi.org/10.1063/5.0147435>

INTRODUCTION

The kesterite phase of the quaternary semiconductor $\text{Cu}_2\text{ZnSnS}_4$ (CZTS) has been identified as a promising low-cost absorber material for thin-film solar cells.^{1,2} Its non-toxic and earth-abundant elemental composition makes it an attractive candidate compared to alternatives such as CdTe and Cu(In,Ga)Se₂ (CIGS) solar cells, which face toxicity issues and material scarcity.^{3–6} It is reported that CZTS has a direct bandgap of about 1.5 eV, which is close to the optimum single-junction value.⁷ However, the power conversion efficiency record of CZTS is far lower than that of the CdTe and CIGS thin film solar cells.^{8–10} This deficiency has been attributed to issues including low open circuit voltage,^{11,12} Cu–Zn disorder,^{13,14} and, particularly, the detrimental properties of grain boundaries (GBs).^{15,16}

More generally, GBs are commonly associated with enhanced carrier recombination and reduced efficiency due to deep trap states induced by unavoidable dangling bonds and segregation of point defects.^{17–20} Although GBs are widely observed in CZTS films,^{21–23} direct information on their structure and electronic properties that can be invaluable for optimizing material

performance remains scarce. Theoretical studies are also relatively uncommon and challenging as direct information on the atomic scale structure of GBs in CZTS is not available from experiments. Previous first-principles simulations have mainly focused on the electronic properties of $\Sigma 3$ (114) GBs,^{24–26} with structures obtained through the cation mutation of similar GBs in CdTe and CuInSe₂. A more recent study also considered $\Sigma 3$ (112) GBs in CZTS,²⁷ which, if present, would be expected to separate grains along the growth direction due to the preferential (112) grain texture of CZTS thin films.²¹ However, columnar growth is usually observed in thin films where GBs are more likely to form on planes perpendicular (or near-perpendicular) to the preferred (112) grain texture, which is not the case for any of the previously studied GB types. Therefore, predictive modeling of other GB types in CZTS is urgently needed to better understand their effects in real films.

A second challenge to modeling GBs in CZTS is that the large supercell sizes required often prohibit full geometry optimization and electronic structure calculation using the hybrid functionals, such as HSE06,²⁸ which has been shown to predict the structure and bandgap of CZTS in good agreement with experiments. A common approach to this issue is structural optimization using

computationally cheaper semi-local approximations to exchange and correlation, e.g., generalized gradient approximations (GGAs), followed by the calculation of electronic properties using the accurate hybrid HSE06 functional.²⁸ However, recent reports have shown that this yields significant errors in structures and bandgaps for CZTS.^{29–31} Thus, an accurate simulation of GBs with an affordable approach remains a challenge.

In this article, we tackle the challenges identified above by employing first-principles simulations to predict the structure of two previously unstudied GB orientations in CZTS and investigate their electronic properties. The MS2 meta-GGA functional is used for geometry optimization followed by the calculation of electronic properties with HSE06, which, as shown previously, yields accurate structures and bandgaps for bulk CZTS.³⁰ We identify four new CZTS GBs with low formation energies: two $\Sigma 3$ (111) (Zn–Zn core and S–S core) and two $\Sigma 5$ (201) (Cu + Zn core and S–S core). Analysis of their electronic structures indicates that one $\Sigma 3$ (111) GB and one $\Sigma 5$ (201) GB should be electronically benign as no deep trap states are present. We also consider defect segregation behavior in all new GBs, and the results show that an easily formed Cu-poor (Zn-rich) environment in the $\Sigma 3$ (111) GB (S–S core) is reported to be beneficial according to the previous experimental results. Our work not only enriches the CZTS GB family, but also provides a deep insight into how to explore new GBs from simulations.

METHODS

First-principles density functional theory (DFT) calculations using the projected augmented-wave method (PAW) were performed using the Vienna *ab initio* simulation package (VASP).^{32,33} An energy cutoff of 400 eV for the plane wave basis set was used throughout all calculations. The atomic structure of all GB models was carefully optimized with the MS2 meta-GGA functional³⁴ since it has been proven to give much more accurate structures for bulk CZTS ($a = 5.40$ Å, $c = 10.84$ Å) compared to other GGA or meta-GGA functionals.³⁰ Total energies were converged to 10^{-5} eV and structures optimized until all atomic forces were less than 0.01 eV Å⁻¹. A reduced k -point mesh of $3 \times 3 \times 1$ for $\Sigma 3$ (111) GBs and $5 \times 1 \times 1$ for $\Sigma 5$ (201) GBs was used during geometry optimization. For a more accurate prediction of GB/defect energy levels and band edge positions, the electronic properties are recomputed using the hybrid HSE06 functional (using the gamma-point only) based on the MS2-optimized structures.

All GBs were constructed based on slab models with free surfaces terminated with pseudo-hydrogen to prevent unphysical charge transfer. Pseudo-hydrogen with fractional charge $\alpha = (8 - Z)/4$ (where Z is the valence electron of the atom in the compound) was used according to the passivation scheme proposed by Wang *et al.*,³⁵ which has been successfully applied to other tetrahedral semiconductors.³⁶ In this case, the fractional charge α used for Cu, Zn, Sn, and S was 1.75, 1.5, 1.0, and 0.5 e, respectively. To prevent interactions between adjacent supercells, a minimum of 10 Å vacuum spacing between free surfaces was maintained. The optimized lattice constants for $\Sigma 3$ (111) GBs are $a = 7.63$ Å, $b = 12.11$ Å, and $c = 64.15$ Å and for $\Sigma 5$ (201) GBs are $a = 5.39$ Å, $b = 22.34$ Å, and $c = 49.78$ Å.

RESULTS AND DISCUSSION

We consider two low-index orientations that are perpendicular to the experimentally observed (112) film texture²¹ as model GB planes that may separate columnar grains in CZTS films: $\Sigma 3$ (111) and $\Sigma 5$ (201). For each GB orientation, we consider two possible mirror symmetric grain terminations: Cu + Zn-rich termination created by adjoining two Cu + Zn terminated grains and S-rich termination created by adjoining two S terminated grains. To identify stable rigid body translations, we construct stoichiometric periodic supercells for each orientation with both Cu + Zn-rich and S-rich GBs separated by at least 27 Å to minimize interactions between periodically repeated images. Following the gamma surface approach,³⁷ we optimize all configurations for rigid body translations parallel to the GB plane in 1 Å intervals in both x and y directions and perpendicular to the GB plane in 0.5 Å intervals in the z direction. Initially, the MS2 functional with an increased energy tolerance of 10^{-4} eV is used for geometry optimization to save the computational cost. Figures 1(a) and 1(b) show the corresponding gamma surfaces with the most stable translation states identified as (0, 0, 1) and (0, 6, 0.5) Å for $\Sigma 3$ (111) and $\Sigma 5$ (201) GB supercells, respectively. The most stable structures are then re-optimized using the MS2 functional and tighter energy tolerance (namely, 10^{-5} eV) yielding the structures shown in Figs. 1(c) and 1(d). The corresponding GB formation energies are calculated as follows:

$$E_f = \frac{E_{GB} - N \times E_{bulk}}{2A},$$

where E_{GB} is the total energy of the GB supercell, E_{bulk} is the energy per formula unit of bulk CZTS, N is the number of CZTS formula units in the GB supercell, and A is the cross-sectional GB area. The calculated formation energies for $\Sigma 3$ (111) and $\Sigma 5$ (201) GBs are 0.83 and 1.35 Jm⁻², indicating that they are energetically stable (similar to that of the more widely studied $\Sigma 3$ (112) and $\Sigma 3$ (114) GBs). However, since the supercells contain two GBs, their formation energies represent an average of both terminations.

To address the properties of individual GB terminations, a different approach is required. Based on the structures obtained above, we construct four new GB supercells, each containing only a single GB and two free surfaces separated by a vacuum gap. The free surfaces are passivated using a pseudo-hydrogen approach as described in the Methods section, and the supercells are fully re-optimized using the MS2 functional. In the following, we refer to these four GB models as GB1 [$\Sigma 3$ (111) Zn–Zn core], GB2 [$\Sigma 3$ (111) S–S core], GB3 [$\Sigma 5$ (201) Cu + Zn core], and GB4 [$\Sigma 5$ (201) S–S core]. Figures 2(a)–2(d) show the atomic structure of these four models in the vicinity of the GB, while their full configurations are shown in Fig. S1 in the supplementary material. The structures of single-GB supercell models are found to be very consistent with that of double-GB supercell models (differences in bond lengths near the GB less than 0.1 Å).

Examining the structures of $\Sigma 3$ (111) GBs in CZTS, we find a short Zn–Zn bond (2.280 Å) in the Zn–Zn core GB (GB1). This shares some similarities with $\Sigma 3$ (112) GBs of binary chalcogenide CdTe.³⁸ However, unlike CdTe, the corresponding S–S core GB

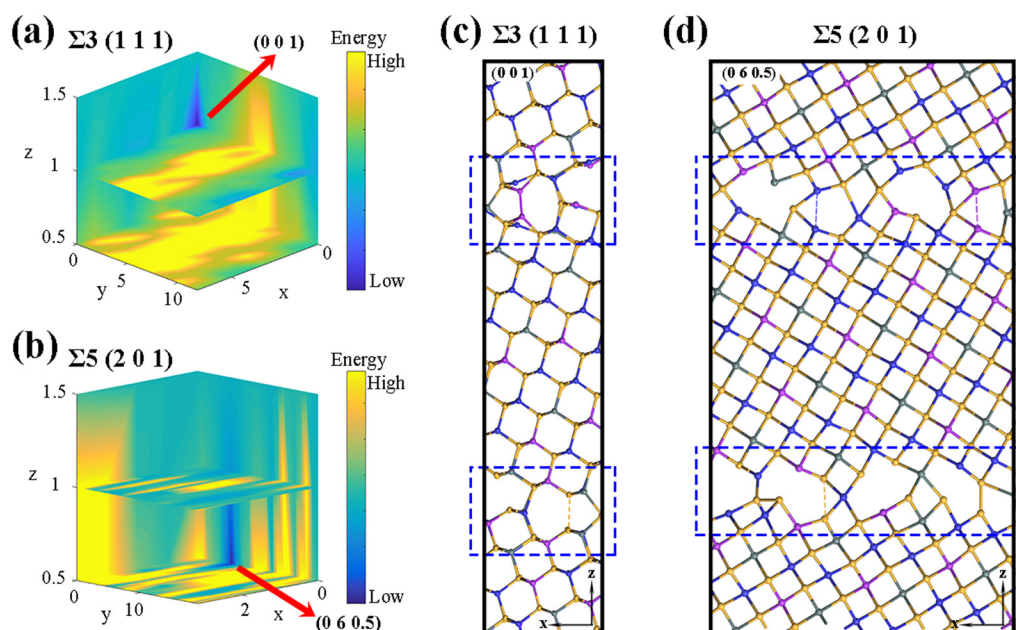


FIG. 1. Gamma surfaces showing how the GB formation energy varies with rigid body translation for (a) $\Sigma 3$ (111) and (b) $\Sigma 5$ (201) GB supercells. The most stable translation states are identified as (0, 0, 1) and (0, 6, 0.5) Å for $\Sigma 3$ (111) and $\Sigma 5$ (201) GB supercells, respectively, and the corresponding structures optimized with the MS2 functional are shown in (c) $\Sigma 3$ (111) and (d) $\Sigma 5$ (201). The configurations of the GB area are highlighted with blue dashed lines. Blue, purple, gray, and yellow balls represent Cu, Zn, Sn, and S atoms, respectively.

(GB2) has no short S–S bonds (the shortest S–S bonds are 3.204 and 3.263 Å). For $\Sigma 5$ (201) GBs in CZTS, we find weak Zn–Zn (2.776 Å) and strong Cu–Cu bonds (2.648 Å) present in the Cu + Zn core GB (GB3), albeit longer than in the case for GB1. For the S–S core GB (GB4), several short S–S bonds are present (2.183, 2.228, and 2.903 Å).

We will now turn to address the electronic properties of the GB models described above. However, we would first like to highlight how the approach used for optimizing the GB structures can have a significant effect on the results obtained. The large supercell sizes involved in GB modeling make full geometry optimization using the accurate hybrid HSE06 functional prohibitively expensive in terms of computational cost. The commonly employed alternative is to optimize the structure using a GGA functional (e.g., PBE) followed by the calculation of electronic properties using HSE06 but without geometry optimization. However, previous studies have shown that this can lead to significant errors in the determination of the bulk bandgap of CZTS due to the inaccurate prediction of Sn–S bond lengths by PBE.²⁹ Our previous work³⁰ has shown that the MS2 functional yields a more accurate Sn–S bond length (2.436 Å) and, therefore, a more accurate basis for electronic structure calculations using HSE06. To further confirm whether the MS2 functional also works well in CZTS GBs, we have performed equivalent GB structure optimizations using the PBE functional to allow comparison, with key results summarized in Table I. We find that for all MS2-optimized GBs, the Sn–S bond length in the center of the grains (see Fig. S1 in the supplementary material for definition) is

very close to that of the bulk crystal (2.41 ± 0.01 Å from experiment³⁹ and 2.418 Å from DFT using HSE06),³⁰ whereas in the PBE-optimized GBs, the Sn–S bond length is around 0.02 Å longer. While a small increase leads to a 0.1 eV predicted decrease in the bandgap of CZTS.^{29,30} More significantly, single point energy calculations with the HSE06 functional show that MS2-optimized GB structures are significantly more stable than those optimized with PBE. For each GB, the HSE06 computed energy difference between PBE and MS2 optimized structures (ΔE) ranges from -0.74 to -0.29 eV (Table I). There are also significant differences in the structure near the GB with the S–S dangling bond in GB2 showing the largest difference of 0.15 Å. Importantly, the negative values of ΔE indicate that all GB structures optimized using the MS2 functional are more energetically stable than those optimized using PBE.

The dangling bonds at GBs identified above have important effects on their electronic properties. As shown in Fig. 2(e), trap states (both shallow and deep) are present in all CZTS GBs due to the complex chemical environment in GB areas, including under-coordinated atoms and dangling bonds. GB1 [$\Sigma 3$ (111) Cu + Zn-rich] has an occupied deep trap associated with the short Zn–Zn dangling bond. Additional shallow occupied hole and electron traps are located above the bulk valence band maximum (VBM) and below the bulk conduction band minimum (CBM), respectively. Further analysis of band decomposed charge densities indicates that these shallow states are delocalized in the vicinity of the GB. GB2 [$\Sigma 3$ (111) S-rich], on the other hand, presents no

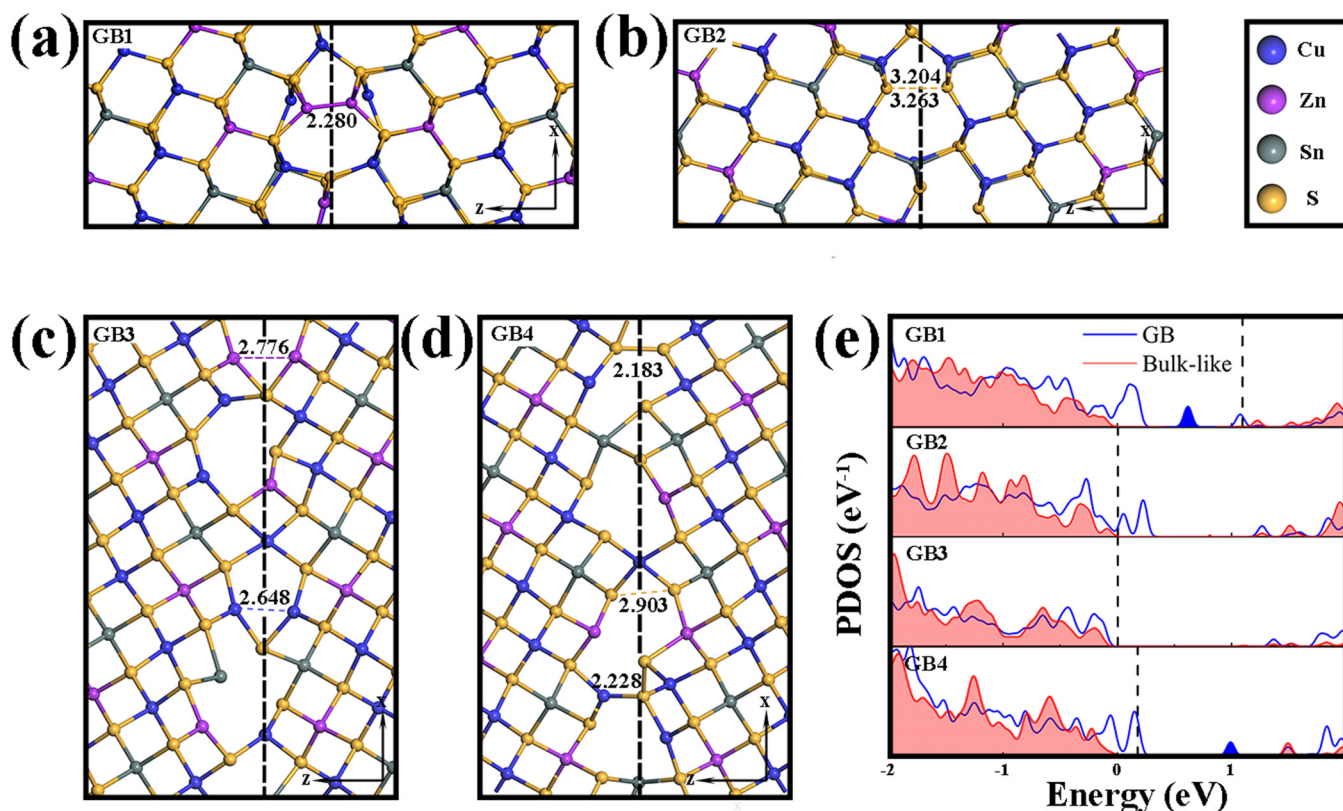


FIG. 2. Relaxed atomic structures of (a) GB1 ($\Sigma 3$ (111) Zn-Zn core), (b) GB2 ($\Sigma 3$ (111) S-S core), (c) GB3 ($\Sigma 5$ (201) Cu + Zn core), and (d) GB4 ($\Sigma 5$ (201) S-S core). Black dashed lines indicate the GB plane. (e) Density of states (calculated using the HSE06 functional) projected in the bulk-like and GB regions of GB1, GB2, GB3, and GB4 (from top to bottom). The zero of the energy scale is set to the valance band maximum of bulk CZTS. The black dashed lines represent the Fermi energy and the blue-shaded peaks highlight the deep trap states. Blue, purple, gray, and yellow balls represent Cu, Zn, Sn, and S atoms, respectively.

deep traps, consistent with the absence of short dangling bonds, but does introduce some similar shallow unoccupied hole traps above the bulk VBM. Unexpectedly, GB3 [$\Sigma 5$ (201) Cu + Zn-rich] presents no shallow or deep gap states. This suggests that the relatively short Zn-Zn (2.776 Å) and Cu-Cu bonds (2.648 Å) are benign in terms of their effect on the near-gap electronic structure. However, GB4 [$\Sigma 5$ (201) S-rich] has an unoccupied deep gap state

TABLE I. Average Sn-S bond length in the bulk-like area of different GBs after geometry optimization by PBE ($d_{\text{Sn-S-PBE}}$) and MS2 ($d_{\text{Sn-S-MS2}}$) functionals. Total energy difference (ΔE) computed using the HSE06 functional between PBE- and MS2-optimized GB structures. The negative value of ΔE indicates that the GB structure optimized by MS2 is more stable.

GB type	$d_{\text{Sn-S-MS2}}$ (Å)	$d_{\text{Sn-S-PBE}}$ (Å)	ΔE (eV)
GB1	2.435	2.454	-0.54
GB2	2.438	2.453	-0.29
GB3	2.438	2.459	-0.74
GB4	2.436	2.458	-0.51

associated with short S-S bonds and unoccupied shallow hole states near the bulk VBM, but no gap states are found below the bulk CBM. The deep trap states found for GB1 and GB4 would be expected to play a significant role in non-radiative recombination and, therefore, be detrimental to the overall performance of thin film CZTS solar cells. Similar deep trap states have also been reported in GBs of binary and ternary chalcogenide compounds CdTe⁴⁰ and CuInSe₂²⁴ also associated with anion-anion or cation-cation dangling bonds. Among all the GBs considered here, GB3 is the most benign as it shows no GB trap states at all, despite introducing shorter Cu-Cu and Zn-Zn bonds than present in the bulk crystal.

As a quaternary compound, CZTS has many possible intrinsic point defects, such as vacancies (V_{Cu} , V_{Zn} , V_{Sn} , and V_{S}), interstitials (Cu_i , Zn_i , Sn_i , and S_i), and antisites (Cu_{Zn} , Zn_{Cu} , Sn_{Zn} , and Zn_{Sn}). The stability and electronic properties of such defects play a key role in the formation of secondary phases, Cu-Zn disorder, and, ultimately, the efficiency of CZTS solar cells.^{41,42} Among all possible intrinsic defects, cation antisite defects have been reported to have low formation energy in bulk CZTS.⁴³ However, their behavior in GBs has not been well explored. Point defects often

segregate to GBs where they may be harmful to material performance (e.g., increased non-radiative recombination) or in some cases beneficial (e.g., due to the elimination of dangling bonds and associated deep gap states).⁴⁴ To provide insight into defect segregation behavior in the four new CZTS GBs identified above, we consider the segregation energy and electronic properties of four typical cation antisite defects (namely, Cu_{Zn} , Zn_{Cu} , Cu_{Sn} , and Sn_{Cu}). Here, we introduce point defects in a neutral charge with respect to the pristine GB model. However, defects will adopt a charge state self-consistent with the Fermi level for the GB [see Fig. 3(e)]. For example, donor defects may become ionized and increase the carrier concentration in an *n*-type GB.

The segregation energy is calculated as the energy difference between a configuration with the point defect in the center of one of the grains (i.e., corresponding to a bulk-like region) and the most stable defect in the GB region (such that negative segregation energies represent favorable segregation to the GB). All possible defect sites in the GB are considered in order to identify the most stable. Segregation energies are calculated using the HSE06 functional with structures obtained by geometry optimization with the MS2 functional. The results are summarized in Fig. 3, with further details given in Table S1 in the [supplementary material](#).

In the majority of cases, defects are found to preferentially segregate to all GBs considered. The driving force for segregation is particularly strong for Cu_{Sn} and Sn_{Cu} defects with segregation energies below -1 eV in all but one anomalous case (Cu_{Sn} in GB2). The most preferential segregation sites of Cu_{Sn} and Sn_{Cu} are both junction points that connect to two grains. As for Cu_{Zn} and Zn_{Cu} defects, no strong driving force for segregation behavior has been found in all GB models since the absolute values of their segregation energies are no more than 0.5 eV, except for one anomalous case (Zn_{Cu} in GB2). A deeper insight into the anomalous cases in

GB2 will be provided in the following section. The low formation energy of Cu_{Zn} and Zn_{Cu} antisites means they are common defects in CZTS and responsible for the observed Cu–Zn disorder. However, the segregation energies of Cu_{Zn} and Zn_{Cu} antisites to a given GB are often found to be quite different, which means one may expect local variations in Cu–Zn stoichiometry at GBs. Furthermore, such variations in stoichiometry can be different for different GB types (e.g., Zn-rich in the case of GB1 and GB2 and Cu-rich in the case of GB4). Such heterogeneity of GB properties will present a serious obstacle to the passivation of GB defects in order to optimize CZTS for solar cell applications.

On the other hand, previous works have shown that in some cases, rather than being a hindrance, the segregation of point defects to GBs can help passivate GBs by removing deep trap states associated with dangling bonds.^{45,46} GB1 and GB4 (Fig. 2) provide two examples of GBs with deep states associated with dangling bonds (Zn–Zn in GB1 and S–S in GB4), as one might not expect any of the cation antisite defects considered to remove the S–S dangling bond in GB4. However, the Zn–Zn dangling bond is broken by the segregation of Cu_{Zn} (which as noted previously, is a defect with low formation energy) to GB1 and the deep gap state is removed as shown in Fig. S2 in the [supplementary material](#). Thus, once intrinsic cation antisite defects are taken into account, only GB4 remains as problematic with respect to deep gap states. To passivate this GB, other intrinsic defects on the anion sublattice or extrinsic dopants would be needed.

It should be noted that among all GBs, GB2 shows an abnormal defect segregation behavior. First, as mentioned before, the Cu_{Sn} defect exhibits a positive segregation energy in GB2, which means this defect favors bulk regions, leaving the GB in a Cu-poor environment. Second, the Zn_{Cu} antisite shows an unusual strong negative segregation energy in GB2, which indicates that such a defect prefers locating at the GB area, leaving the GB in a Zn-rich environment. All these results clearly show that GB2 would easily become Zn-rich and Cu-poor based on the low formation energy of these defects. Previous works^{47–50} have reported that such a Zn-rich (Cu-poor) environment is particularly beneficial for CZTS solar cell efficiency. Indeed, the GB projected density of states (Fig. S3 in the [supplementary material](#)) shows that no additional trap states are introduced when the Zn_{Cu} antisite segregates to GB. Therefore, GB2 remains benign even in the presence of intrinsic antisite defects.

To understand why Cu_{Sn} and Zn_{Cu} exhibit such abnormal defect segregation behavior, a more detailed analysis is employed. Figures 4(a) and 4(c) show the segregation energy (with respect to the site in the center of the grain) for $\text{Cu}_{\text{Sn}}/\text{Zn}_{\text{Cu}}$ antisite defects in the vicinity of GB2. Figures 4(b) and 4(d) show the atomic structure of GB2 when the $\text{Cu}_{\text{Sn}}/\text{Zn}_{\text{Cu}}$ antisite defect is located at the GB core, namely, site Sn0/Cu0 (other sites of Sn/Cu are also labeled). The Zn_{Cu} defect clearly prefers segregating to the GB region over the bulk, with a gradual decrease in energy over a wide region up to 16 Å from the GB core. The opposite is true for Cu_{Sn} . The variation in energy for the Cu_{Sn} defect is relatively small (no more than 0.05 eV) except for a narrow region ± 4 Å from the GB core where the energy sharply increases by ~ 0.4 eV [Fig. 4(a)]. This indicates that the Cu_{Sn} antisite would be easily repelled from the GB, leaving the GB and grain in a different chemical environment.

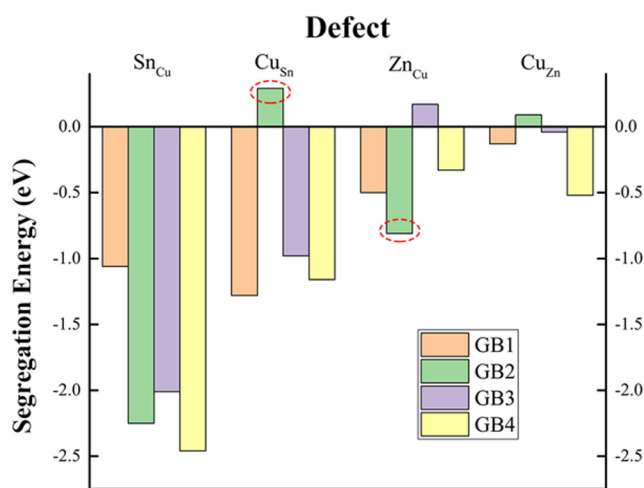


FIG. 3. Segregation energy of Cu_{Zn} , Zn_{Cu} , Cu_{Sn} , and Sn_{Cu} to different GBs. The red dashed circle represents an anomalous defect segregation behavior in GB2. All segregation energies are calculated using the HSE06 functional with structures obtained by geometry optimization with the MS2 functional.

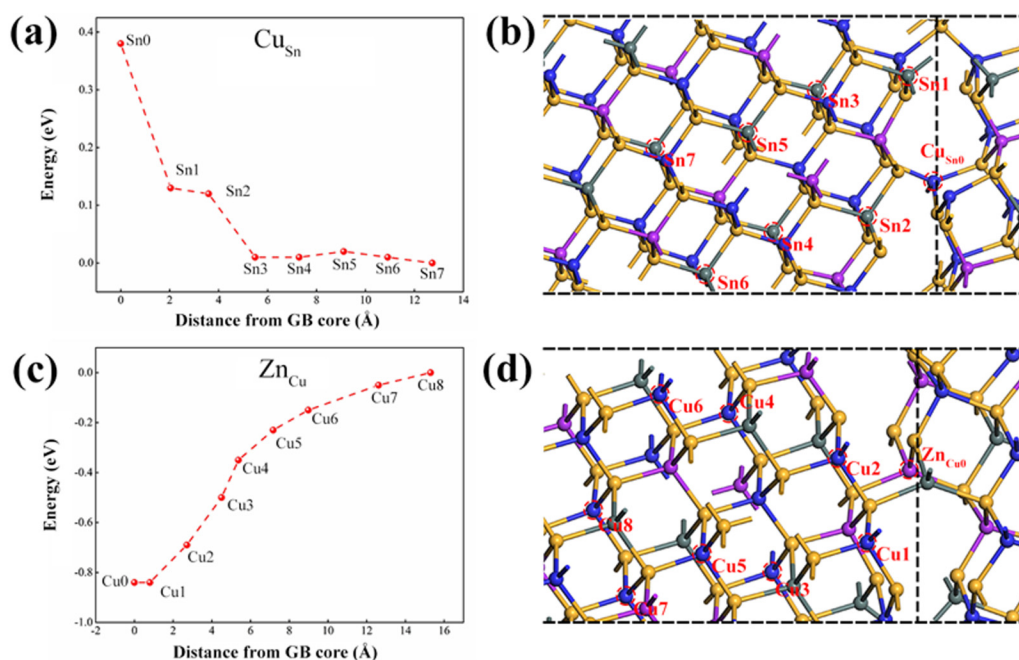


FIG. 4. Energy distribution of the antisite defect (a) Cu_{Sn} and (c) Zn_{Cu} occurring at different sites highlighted in (b) and (d). All single point energies are calculated using the HSE06 functional with structures obtained by geometry optimization with the MS2 functional. (b) Cu_{Sn} appears at the GB core, namely, site Sn0; (d) Zn_{Cu} appears at the GB core, namely, site Cu0.

The different segregation behavior between Zn_{Cu} and Cu_{Sn} defects can be explained by the fact that the former is a donor while the latter is an acceptor. As aforementioned, there are two under-coordinated S atoms in the GB. Each of them needs to gain more electrons to satisfy the electron counting rule. This naturally favors the segregation of donor-like defects (such as Zn_{Cu}) over acceptor-like defects (such as Cu_{Sn}). The net result is that GB2 is predicted to readily adopt a Zn-rich and Cu-poor environment in the presence of intrinsic defects, which is beneficial for its performance.^{47–50}

A complete study of all possible charge states would be a natural and important extension to this work. Although this is non-trivial, as accessing all charge states of a defect by modifying the Fermi energy would also be expected to cause significant effects on the electronic and structural properties of the GB itself (for example, populating or depopulating the deep trap states associated with dangling/wrong bonds). Therefore, separating the properties of the GB and associated point defects is a challenging problem.

CONCLUSIONS

In summary, using density functional theory simulations, we have systematically studied several previously unexplored GBs in CZTS. First, it is confirmed that the new meta-GGA functional MS2 is superior to the traditional GGA method PBE for modeling the structure of GBs in CZTS. Second, four new stable GBs,

including two $\Sigma 3$ (111) and two $\Sigma 5$ (201) GBs, have been modeled for the first time, providing an insight into the diverse atomic structures of CZTS GBs. Third, it is revealed that as for GBs in other chalcogenide compounds (including binary CdTe, ternary CuInSe), only strong cation–cation or anion–anion strong dangling bonds induce detrimental deep trap states. One of the $\Sigma 5$ (201) GBs is predicted to be particularly benign with no trap states in the bandgap, but others exhibit a mix of shallow and deep trap states. These intricate electronic properties of CZTS GBs come from their inherent complex structure, leading to varied GB structures. Further analysis indicates that one of the $\Sigma 3$ (111) GBs is also relatively benign due to (1) the presence of only shallow GB states and no deep trap states and (2) an abnormal defect segregation behavior that leads to a Cu-poor (Zn-rich) GB composition, which is reported to be beneficial according to the previous experimental results.^{47–50} However, taken together, our results indicate that the passivation of all GB types in CZTS will be challenging due to their varied properties. This would require careful control of intrinsic and extrinsic defects as well as the microstructure and is an important topic of further research.

SUPPLEMENTARY MATERIAL

See the [supplementary material](#) for full relaxed configuration of $\Sigma 3$ (111) and $\Sigma 5$ (201) GBs and segregation energies of all defects at different sites in all GBs.

ACKNOWLEDGMENTS

C.-J.T. acknowledges support by the National Natural Science Foundation (No. 12104515). N.-J.H. and R.-X.D. acknowledge support from National College Students' innovation and entrepreneurship training program (No. 2022105330185). K.P.M. acknowledges support from EPSRC (Nos. EP/K003151/1, EP/P006051/1, and EP/P023843/1). This work made use of the facilities of Archer, the United Kingdom's national high-performance computing service, via our membership in the UK HPC Materials Chemistry Consortium, which is funded by EPSRC (Nos. EP/L000202/1 and EP/R029431/1). This project also made use of the Viking Cluster, which is a high-performance computation facility provided by the University of York. We are grateful for resources from the High-Performance Computing Center of Central South University and Hefei Advanced Computing Center. All data created during this research are available by request from the University of York Research database at <https://doi.org/10.15124/32b9075-80ee-4f08-b93c-53f2398d7c84>.

AUTHOR DECLARATIONS

Conflict of Interest

The authors have no conflicts to disclose.

Author Contributions

Ning-Jing Hao: Formal analysis (equal); Investigation (equal); Writing – original draft (equal). **Rui-Xue Ding:** Formal analysis (equal); Investigation (equal); Writing – original draft (equal). **Chuan-Jia Tong:** Conceptualization (equal); Data curation (equal); Formal analysis (equal); Investigation (equal); Methodology (equal); Supervision (equal); Validation (equal); Visualization (equal); Writing – original draft (equal); Writing – review & editing (equal). **Keith P. McKenna:** Conceptualization (equal); Data curation (equal); Formal analysis (equal); Funding acquisition (equal); Investigation (equal); Methodology (equal); Project administration (equal); Resources (equal); Supervision (equal); Validation (equal); Visualization (equal); Writing – original draft (equal); Writing – review & editing (equal).

DATA AVAILABILITY

All data created during this research are available by request from the University of York Research database at TBC.

REFERENCES

- M. Graetzel, R. A. J. Janssen, D. B. Mitzi, and E. H. Sargent, "Materials interface engineering for solution-processed photovoltaics," *Nature* **488**, 304 (2012).
- K.-J. Yang, S. Kim, S.-Y. Kim, K. Ahn, D.-H. Son, S.-H. Kim, S.-J. Lee, Y.-I. Kim, S.-N. Park, S.-J. Sung, D.-H. Kim, T. Enkhbat, J. Kim, C.-W. Jeon, and J.-K. Kang, "Flexible $\text{Cu}_2\text{ZnSn}(\text{S},\text{Se})_4$ solar cells with over 10% efficiency and methods of enlarging the cell area," *Nat. Commun.* **10**, 2959 (2019).
- C. Yan, J. Huang, K. Sun, S. Johnston, Y. Zhang, H. Sun, A. Pu, M. He, F. Liu, K. Eder, L. Yang, J. M. Cairney, N. J. Ekins-Daukes, Z. Hameiri, J. A. Stride, S. Chen, M. A. Green, and X. Hao, " $\text{Cu}_2\text{ZnSnS}_4$ solar cells with over 10% power conversion efficiency enabled by heterojunction heat treatment," *Nat. Energy* **3**, 764 (2018).

- K. Kaur, N. Kumar, and M. Kumar, "Strategic review of interface carrier recombination in earth abundant Cu–Zn–Sn–S–Se solar cells: Current challenges and future prospects," *J. Mater. Chem. A* **5**, 3069 (2017).
- D. Shin, B. Saparov, and D. B. Mitzi, "Defect engineering in multinary earth-abundant chalcogenide photovoltaic materials," *Adv. Energy Mater.* **7**, 1602366 (2017).
- N. Khemiri, S. Chamekh, and M. Kanzari, "Properties of thermally evaporated CZTS thin films and numerical simulation of earth abundant and non toxic CZTS/Zn(S,O) based solar cells," *Solar Energy* **207**, 496 (2020).
- S. C. Riha, B. A. Parkinson, and A. L. Prieto, "Solution-based synthesis and characterization of $\text{Cu}_2\text{ZnSnS}_4$ nanocrystals," *J. Am. Chem. Soc.* **131**, 12054 (2009).
- M. He, C. Yan, J. Li, M. P. Suryawanshi, J. Kim, M. A. Green, and X. Hao, "Kesterite solar cells: Insights into current strategies and challenges," *Adv. Sci.* **8**, 2004313 (2021).
- A. Chirilă, P. Reinhard, F. Pianezzi, P. Bloesch, A. R. Uhl, C. Fella, L. Kranz, D. Keller, C. Gretener, H. Hagendorfer, D. Jaeger, R. Erni, S. Nishiwaki, S. Buecheler, and A. N. Tiwari, "Potassium-Induced surface modification of Cu(In,Ga)Se₂ thin films for high-efficiency solar cells," *Nat. Mater.* **12**, 1107 (2013).
- A. Hu, J. Zhou, P. Zhong, X. Qin, M. Zhang, Y. Jiang, X. Wu, and D. Yang, "High-efficiency CdTe-based thin-film solar cells with ultrathin CdS:O window layer and processes with post annealing," *Solar Energy* **214**, 319 (2021).
- J.-S. Park, J.-H. Yang, A. Kanevce, S. Choi, I. L. Repins, and S.-H. Wei, "Ordering-induced direct-to-indirect band Gap transition in multication semiconductor compounds," *Phys. Rev. B* **91**, 075204 (2015).
- Q. Zhao, H. Shen, Y. Xu, K. Gao, D. Chen, and Y. Li, "Effect of CZTS/CCZTS stacked structures prepared through split-cycle on the performance of flexible solar cells," *ACS Appl. Energy Mater.* **5**, 3668 (2022).
- J. K. Larsen, J. J. S. Scragg, N. Ross, and C. Platzer-Björkman, "Band tails and Cu–Zn disorder in $\text{Cu}_2\text{ZnSnS}_4$ solar cells," *ACS Appl. Energy Mater.* **3**, 7520 (2020).
- E. Isotta, U. Syafiq, N. Ataollahi, A. Chiappini, C. Malerba, S. Luong, V. Trifiletti, O. Fenwick, N. M. Pugno, and P. Scardi, "Thermoelectric properties of CZTS thin films: Effect of Cu–Zn disorder," *Phys. Chem. Chem. Phys.* **23**, 13148 (2021).
- M. Kumar, A. Dubey, N. Adhikari, S. Venkatesan, and Q. Qiao, "Strategic review of secondary phases, defects and defect-complexes in kesterite CZTS–Se solar cells," *Energy Environ. Sci.* **8**, 3134 (2015).
- J. Li, D. B. Mitzi, and V. B. Shenoy, "Structure and electronic properties of grain boundaries in earth-abundant photovoltaic absorber $\text{Cu}_2\text{ZnSnSe}_4$," *ACS Nano* **5**, 8613 (2011).
- T. S. Sherkar, C. Momblona, L. Gil-Escrig, J. Àvila, M. Sessolo, H. J. Bolink, and L. J. A. Koster, "Recombination in perovskite solar cells: Significance of grain boundaries, interface traps, and defect ions," *ACS Energy Lett.* **2**, 1214 (2017).
- Y. Ma, W. Li, Y. Feng, Z. Li, X. Ma, X. Liu, X. Wu, Y. Zhang, C. Yang, X. Lu, K. Wang, and X. Xiao, "Band bending near grain boundaries of $\text{Cu}_2\text{ZnSn}(\text{S},\text{Se})_4$ thin films and Its effect on photovoltaic performance," *Nano Energy* **51**, 37 (2018).
- D. Savchenko, V. Rodionov, A. Prokhorov, J. Lančok, E. Kalabukhova, and B. Shanina, "Impact of the dangling bond defects and grain boundaries on trapping recombination process in polycrystalline 3C SiC," *J. Alloys Compd.* **823**, 153752 (2020).
- B. G. Mendis, K. P. McKenna, G. Gurieva, M. S. Rumsey, and S. Schorr, "Crystal structure and anti-site boundary defect characterisation of $\text{Cu}_2\text{ZnSnSe}_4$," *J. Mater. Chem. A* **6**, 189 (2018).
- W. M. Hlaing Oo, J. L. Johnson, A. Bhatia, E. A. Lund, M. M. Nowell, and M. A. Scarpulla, "Grain size and texture of $\text{Cu}_2\text{ZnSnS}_4$ thin films synthesized by cosputtering binary sulfides and annealing: Effects of processing conditions and sodium," *J. Electron. Mater.* **40**, 2214 (2011).

- ²²M. J. Romero, H. Du, G. Teeter, Y. Yan, and M. M. Al-Jassim, "Comparative study of the luminescence and intrinsic point defects in the kesterite $\text{Cu}_2\text{ZnSnS}_4$ and chalcopyrite $\text{Cu}(\text{In,Ga})\text{Se}_2$ thin films used in photovoltaic applications," *Phys. Rev. B* **84**, 165324 (2011).
- ²³J. B. Li, V. Chawla, and B. M. Clemens, "Investigating the role of grain boundaries in CZTS and CZTSSe thin film solar cells with scanning probe microscopy," *Adv. Mater.* **24**, 720 (2012).
- ²⁴C.-Y. Liu, Z.-M. Li, H.-Y. Gu, S.-Y. Chen, H. Xiang, and X.-G. Gong, "Sodium passivation of the grain boundaries in CuInSe_2 and $\text{Cu}_2\text{ZnSnS}_4$ for high-efficiency solar cells," *Adv. Energy Mater.* **7**, 1601457 (2017).
- ²⁵Z.-Y. Zhao and X. Zhao, "First-principles study on doping effects of sodium in kesterite $\text{Cu}_2\text{ZnSnS}_4$," *Inorg. Chem.* **53**, 9235 (2014).
- ²⁶W.-J. Yin, Y. Wu, S.-H. Wei, R. Noufi, M. M. Al-Jassim, and Y. Yan, "Engineering grain boundaries in $\text{Cu}_2\text{ZnSnSe}_4$ for better cell performance: A first-principle study," *Adv. Energy Mater.* **4**, 1300712 (2014).
- ²⁷M. Wong, K. Tse, and J. Zhu, "New types of CZTS $\Sigma 3$ {112} grain boundaries algorithms to passivation," *J. Phys. Chem. C* **122**, 7759 (2018).
- ²⁸J. Heyd, G. E. Scuseria, and M. Ernzerhof, "Erratum: 'Hybrid functionals based on a screened Coulomb potential' [J. Chem. Phys. **118**, 8207 (2003)]," *J. Chem. Phys.* **124**, 219906 (2006).
- ²⁹J.-S. Park, S. Kim, S. N. Hood, and A. Walsh, "Open-circuit voltage deficit in $\text{Cu}_2\text{ZnSnS}_4$ solar cells by interface bandgap narrowing," *Appl. Phys. Lett.* **113**, 212103 (2018).
- ³⁰C.-J. Tong, H. J. Edwards, T. D. C. Hobson, K. Durose, V. R. Dhanak, J. D. Major, and K. P. McKenna, "Density functional theory and experimental determination of band gaps and lattice parameters in kesterite $\text{Cu}_2\text{ZnSn}(\text{SxSe}_{1-x})_4$," *J. Phys. Chem. Lett.* **11**, 10463 (2020).
- ³¹A. Nagoya, R. Asahi, and G. Kresse, "First-principles study of $\text{Cu}_2\text{ZnSnS}_4$ and the related band offsets for photovoltaic applications," *J. Phys.: Condens. Matter* **23**, 404203 (2011).
- ³²P. E. Blochl, "Projector augmented-wave method," *Phys. Rev. B* **50**, 17953 (1994).
- ³³G. Kresse, "From ultrasoft pseudopotentials to the projector augmented-wave method," *Phys. Rev. B* **59**, 1758 (1999).
- ³⁴J. Sun, B. Xiao, Y. Fang, R. Haunschild, P. Hao, A. Ruzsinszky, G. I. Csonka, G. E. Scuseria, and J. P. Perdew, "Density functionals that recognize covalent, metallic, and weak bonds," *Phys. Rev. Lett.* **111**, 106401 (2013).
- ³⁵J. Li and L.-W. Wang, "Band-structure-corrected local density approximation study of semiconductor quantum dots and wires," *Phys. Rev. B* **72**, 125325 (2005).
- ³⁶H.-X. Deng, S.-S. Li, J. Li, and S.-H. Wei, "Effect of hydrogen passivation on the electronic structure of ionic semiconductor nanostructures," *Phys. Rev. B* **85**, 195328 (2012).
- ³⁷F. Scholz, "Interfaces in crystalline materials (1996) A. P. Sutton, R. W. Balluffi," *J. Solid State Electrochem.* **1**, 117 (1997).
- ³⁸C.-Y. Liu, Y.-Y. Zhang, Y.-S. Hou, S.-Y. Chen, H.-J. Xiang, and X.-G. Gong, "Self-passivation rule and structure of $\text{cdte } \Sigma 3$ (112) grain boundaries," *Phys. Rev. B* **93**, 205426 (2016).
- ³⁹R. Bacewicz, J. Antonowicz, S. Podsiadlo, and S. Schorr, "Local structure in $\text{Cu}_2\text{ZnSnS}_4$ studied by the xafs method," *Solid State Commun.* **177**, 54 (2014).
- ⁴⁰C.-J. Tong and K. P. McKenna, "Passivating grain boundaries in polycrystalline CdTe ," *J. Phys. Chem. C* **123**, 23882 (2019).
- ⁴¹Z. Chen, P.-Z. Zhang, Y. Zhou, X. Zhang, X. Liu, Z. Hou, J. Tang, and W. Li, "Elucidating the influence of sulfur vacancies on nonradiative recombination dynamics in $\text{Cu}_2\text{ZnSnS}_4$ solar absorbers," *J. Phys. Chem. Lett.* **11**, 10354 (2020).
- ⁴²Y. E. Romanyuk, S. G. Haass, S. Giraldo, M. Placidi, D. Tiwari, D. J. Fermin, X. Hao, H. Xin, T. Schnabel, M. Kauk-Kuusik, P. Pistor, S. Lie, and L. H. Wong, "Doping and alloying of kesterites," *J. Phys. Energy* **1**, 044004 (2019).
- ⁴³S. Chen, X. G. Gong, A. Walsh, and S.-H. Wei, "Defect physics of the kesterite thin-film solar cell absorber $\text{Cu}_2\text{ZnSnS}_4$," *Appl. Phys. Lett.* **96**, 021902 (2010).
- ⁴⁴W.-J. Yin, Y. Wu, R. Noufi, M. Al-Jassim, and Y. Yan, "Defect segregation at grain boundary and its impact on photovoltaic performance of CuInSe_2 ," *Appl. Phys. Lett.* **102**, 193905 (2013).
- ⁴⁵E. Ochoa-Martinez, M. Ochoa, R. D. Ortuso, P. Ferdowsi, R. Carron, A. N. Tiwari, U. Steiner, and M. Saliba, "Physical passivation of grain boundaries and defects in perovskite solar cells by an isolating thin polymer," *ACS Energy Lett.* **6**, 2626 (2021).
- ⁴⁶H.-Y. Gu, W.-J. Yin, and X.-G. Gong, "Defect states and passivation mechanism at grain boundaries of zinc-blende semiconductors," *Semicond. Sci. Technol.* **36**, 045028 (2021).
- ⁴⁷T. K. Todorov, K. B. Reuter, and D. B. Mitzi, "High-efficiency solar cell with earth-abundant liquid-processed absorber," *Adv. Mater.* **22**, E156 (2010).
- ⁴⁸S. Ahmed, K. B. Reuter, O. Gunawan, L. Guo, L. T. Romankiw, and H. Deligianni, "A high efficiency electrodeposited $\text{Cu}_2\text{ZnSnS}_4$ solar cell," *Adv. Energy Mater.* **2**, 253 (2012).
- ⁴⁹W. Li, J. Chen, C. Yan, and X. Hao, "The effect of ZnS segregation on Zn-rich CZTS thin film solar cells," *J. Alloys Compd.* **632**, 178 (2015).
- ⁵⁰W. Xiao, J. N. Wang, X. S. Zhao, J. W. Wang, G. J. Huang, L. Cheng, L. J. Jiang, and L. G. Wang, "Intrinsic defects and Na doping in $\text{Cu}_2\text{ZnSnS}_4$: A density-functional theory study," *Solar Energy* **116**, 125 (2015).